Ⓐ Springer

Impact of mechanical ventilation control strategies based on non-steady-state and steady-state Wells-Riley models on airborne transmission and building energy consumption

SHA Hao-han(沙浩瀚), ZHANG Xin(张鑫), QI Da-hai(戚大海)*

Department of Civil and Building Engineering, Université de Sherbrooke, Sherbrooke J1K 2R1, Canada

© Central South University 2022

Abstract: Ventilation is an effective solution for improving indoor air quality and reducing airborne transmission. Buildings need sufficient ventilation to maintain a low infection risk but also need to avoid an excessive ventilation rate, which may lead to high energy consumption. The Wells-Riley (WR) model is widely used to predict infection risk and control the ventilation rate. However, few studies compared the non-steady-state (NSS) and steady-state (SS) WR models that are used for ventilation control. To fill in this research gap, this study investigates the effects of the mechanical ventilation control strategies based on NSS/SS WR models on the required ventilation rates to prevent airborne transmission and related energy consumption. The modified NSS/SS WR models were proposed by considering many parameters that were ignored before, such as the initial quantum concentration. Based on the NSS/SS WR models, two new ventilation control strategies were proposed. A real building in Canada is used as the case study. The results indicate that under a high initial quantum concentration (e.g., 0.3 q/m^3) and no protective measures, SS WR control underestimates the required ventilation rate. The ventilation energy consumption of NSS control is up to 2.5 times as high as that of the SS control.

Key words: building ventilation; Wells-Riley model; building energy consumption; airborne transmission

1 Introduction

Airborne transmission of respiratory diseases can cause global public health emergencies such as the ongoing COVID-19 pandemic, caused by the severe acute respiratory syndrome coronavirus 2 (SARS-CoV-2). More than 178 million cases of COVID-19 and 3 million deaths have been confirmed from December 2019 to June 2021 [1]. Reducing the spread of COVID-19 is a top priority worldwide and particularly in densely populated cities. Since airborne transmission of COVID-19 was confirmed in April 2021 [2−5], ventilation, as an engineering method, is an effective solution in reducing the spread of COVID-19. MORAWSKA et al [4] suggested that ventilation should be recognized as a means of reducing airborne transmission, and that the ventilation rate should be increased.

There are three types of ventilation in buildings: natural ventilation, mechanical ventilation, and hybrid ventilation (both natural ventilation and mechanical ventilation) [6].

Mechanical ventilation is more widely used in buildings than natural ventilation because it is easier to control, which plays a vital role in reducing airborne transmission [6−7].

Ventilation removes virus-laden droplets suspended in the air. However, determining the ideal ventilation rate becomes a critical problem for mechanical ventilation. On the one hand, the ventilation rate must be high enough to remove the contaminated air. Many previous studies have shown that the common mechanical ventilation system aimed at maintaining indoor air quality (IAQ) cannot reduce the infection risk to an acceptable range, and the ventilation rate must be increased [8 − 10]. On the other hand, maintaining the mechanical ventilation rate very high consumes much more energy. The high ventilation rates not only consume too much electricity to operate the fans, but also increase the cooling and heating related energy consumption when it is too hot or cold outside [9]. Except for healthcare buildings, other non-residential buildings always need to balance the impacts of ventilation between energy consumption and preventing COVID-19 [11].

For achieving a proper engineering control, mathematical models that are used to calculate airborne infection risk are required. The Wells-Riley (WR) model has been extensively used to assess COVID-19 outbreaks, by relating the ventilation rate to infection risk. The WR model, which does not require costly experimental and on-site studies, uses the quantum concept to implicitly consider infectivity [12]. A quantum is defined as the number of infectious airborne particles required to infect a person and can include one or more airborne particles; it can only be obtained by backward calculation from an outbreak case. Furthermore, it is easy to incorporate more influencing factors into the WR model, such as wearing masks and social distancing [13]. AGANOVIC et al [14] modified the WR model to consider the impacts of relative humidity on the infection risk. GUO et al [15] integrated a coefficient, called spatial flow influence factor (SFIF), into the WR model to assess the spatial distribution of infection risk. ZHANG et al [12] used a dilution ratio to modify the WR model for considering the spatial distribution of infection risk. Based on the WR model, many studies have proposed mechanical ventilation system control strategies to reduce the infection

risks of airborne disease. HOU et al [10] suggested that the outdoor ventilation threshold to prevent COVID-19 transmission in a classroom has a 3 − 8 air change rate (ACH) with 500 ppm (parts per million, 10^{-6}) CO_2. Based on a SS WR model, DAI et al [8] recommended a 1200 − 4000 m^3/h ventilation rate per infected individual for up to three hours of exposure. However, the studies that used the WR model for assessing COVID-19 transmission only considered either the NSS or SS conditions but rarely compared them.

Most of the existing studies only utilized the SS WR models for evaluating the risk of COVID-19 or proposing control strategies to reduce the infection risks. Also, although some papers investigated the infection risk under both NSS/SS conditions [12, 16], they do not make a clear comparison highlighting the differences between the NSS/SS WR models in COVID-19. For example, one of the important differences between the NSS/ SS WR models is that the NSS WR model can be affected by the initial virus quantum concentration, but no previous studies discussed this point for COVID-19. Since the SS WR model cannot take the initial virus quantum concentration into consideration, a ventilation control system based on this model may fail to prevent airborne transmission. Therefore, it is essential to quantify the difference between the NSS/SS WR models. The conditions that make the results from the SS WR model acceptable should be investigated. The impacts of the common factors, such as the exposure time and protective measures, on the difference between the NSS/SS WR models should be analyzed. Furthermore, the impact of the difference of these two models on HVAC energy consumption is also unclear due to how the required ventilation rates are calculated. The energy consumption of the HVAC system controlled by the NSS/SS WR models should be evaluated and compared.

In summary, few previous studies conducted a thorough investigation to identify the difference in required ventilation rates between NSS/SS WR models and evaluate the impact of these rates on energy consumption. To fill in this research gap, this study began with the development of the mathematical formulations of the NSS/SS WR models. Using COVID-19 as an example, several factors were integrated in the WR model, such as

the effects of protective measures (i.e., wearing masks and social distancing), initial infection rates, and initial virus quantum concentration. Then, two new ventilation control strategies were developed, based on the NSS/SS WR models and IAQ. A real building was selected for the case study. The building features and measured data from the case study were used to investigate the theoretically required ventilation rates and evaluate the impacts of two new ventilation control strategies on fresh air supply rate and energy consumption.

2 Methodology

2.1 Non-steady-state and steady-state Wells-Riley models

This study aims to use the NSS/SS WR models to control the ventilation rate and reduce the infection risk of COVID-19 to a target value. Figure 1 presents the schematic of the parameters used in the NSS/SS WR models, including the ventilation rate, quantum generation rate, pulmonary rate (breath rate), exposure time, etc. Two common protective measures, wearing masks and social distancing, are considered in both models. This section first presents the NSS/SS WR models. Then, considering that the number of infected occupants and initial quantum concentration are difficult to determine in practice, the initial infection rate and the method to estimate initial quantum concentration from CO_2 are introduced.

Assuming that there is no quantum outdoors, the quantum concentration in the building depends on the quantum generated by people and the quantum loss rate. The quantum concentration is

calculated by [17]:

$$\frac{dC_q}{dt} = \frac{\eta_m Iq}{V} - \lambda_q C_q \tag{1}$$

where C_q is the indoor quantum concentration, q/m³; t is the time, h; η_m is the mask filtration efficiency, %; I is the number of infected individuals; q is the generation rate of virus quanta, q/h; V is the volume of indoor space, m³; λ_q is the first-order loss rate for quanta, h⁻¹, which can be the summed effects of ventilation, deposition onto surfaces, and virus decay [18]. In this study, only the effects of ventilation and deposition on the surfaces due to social distancing were considered [19], which were validated. The other effects, e.g., virus deposition, were not verified and may be negligible compared with the effects of ventilation and deposition [14]. According to Ref. [19], the first-order loss rate for quanta can be ventilation rate, λ, multiplied by a social distancing index (i.e., $\lambda_q = P_d \lambda$).

Assuming the initial quantum concentration is $C_{q,0}$ before people enter the building, Eq. (1) can be solved:

$$C_q(t) = \frac{\eta_m Iq}{\lambda_q V} + e^{-\lambda_q t}\left(C_{q,0} - \frac{\eta_m Iq}{\lambda_q V}\right) \tag{2}$$

When the steady state is achieved, the indoor quantum concentration is:

$$C_q = \frac{\eta_m Iq}{\lambda_q V} \tag{3}$$

According to the WR model, the infection risk, P_I, is related to the amount of inhaled quantum. Therefore, under the exposure time θ, P_I of the susceptible people is:
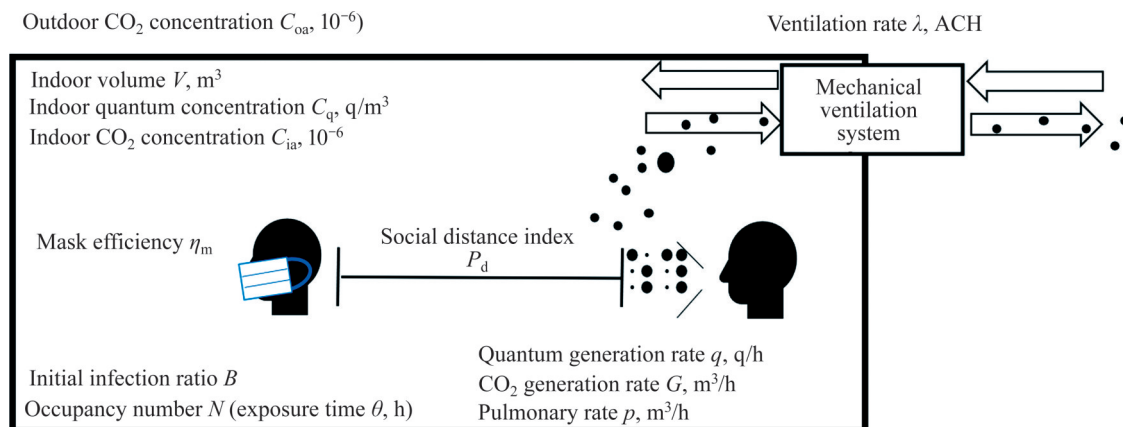

Figure 1 Schematic of parameters used in non-steady-state/steady-state Wells-Riley model for infection risk

$$P_{\mathrm{I}} = 1 - \exp - p\eta_{\mathrm{m}} \int_0^{\theta} C_{\mathrm{q}}(t)\mathrm{d}t \qquad (4)$$

where p is the pulmonary rate, m³/h.

Substituting Eq. (2) and Eq. (3) into Eq. (4), the NSS (Eq. (5a)) and SS WR (Eq. (5b)) models are obtained:

$$P_{\mathrm{I}} = 1 - \exp\left\{ -\frac{\eta_{\mathrm{m}}^2 pIq\theta}{\lambda_{\mathrm{q}}V}\left[1 - \frac{1}{\lambda_{\mathrm{q}}\theta}\left(1 - \mathrm{e}^{-\lambda_{\mathrm{q}}\theta}\right)\cdot \left(1 - \frac{\lambda_{\mathrm{q}}VC_{\mathrm{q},0}}{\eta_{\mathrm{m}}Iq}\right)\right]\right\} \qquad (5a)$$

$$P_{\mathrm{I}} = 1 - \exp\left(-\frac{\eta_{\mathrm{m}}^2 pIq\theta}{\lambda_{\mathrm{q}}V}\right) \qquad (5b)$$

It should be noted that the initial quantum concentration $C_{\mathrm{q},0}$ cannot be measured directly. Considering that the CO_2 is co-exhaled with quantum by the COVID-19 infected individuals, $C_{\mathrm{q},0}$ is estimated by the indoor CO_2 concentration in this study. Many studies have proposed this method of using CO_2 concentration as a substitute for estimating the virus concentration [20 – 22]. When there is no other source generating CO_2, the amount of exhaled CO_2 from all occupants can be calculated through the indoor-outdoor CO_2 concentration difference. When the number of occupants who are infected is known, the exhaled amount of CO_2 and virus from the infected individuals can be estimated. It is easy to calculate the fraction of the CO_2 amount from the infected individuals to the CO_2 from all occupants, which is related to the quantum concentration (See the following Eqs. (6) and (7)).

Considering that indoor air is well mixed at the initial conditions, the indoor and outdoor CO_2 concentration difference, ΔC (i.e., $\Delta C = C_{\mathrm{ia}} - C_{\mathrm{oa}}$), is:

$$\Delta C = \frac{GN}{\lambda V} \qquad (6)$$

where G is the CO_2 generation rate per person, m³/h; N is the number of occupants; λ is the loss rate coefficient of CO_2 (equal to the air change rate). Assuming that the initial infection rate in the population is B (i.e., $I = BN$), with Eq. (3), the relationship between the initial quantum concentration of COVID-19 and CO_2 is described by:

$$C_{\mathrm{q},0} = \frac{\eta_{\mathrm{m}} Bq\Delta C}{P_{\mathrm{d}} G} \qquad (7)$$

Substituting Eq. (7) into Eq. (5a), the NSS WR equation is converted to the following equation.

With the initial infection rate, Eq. (5b) can also be presented as Eq. (8b):

$$P_{\mathrm{I}} = 1 - \exp\left\{ -\frac{\eta_{\mathrm{m}}^2 pBNq\theta}{\lambda_{\mathrm{q}}V}\left[1 - \frac{1}{\lambda_{\mathrm{q}}\theta}\left(1 - \mathrm{e}^{-\lambda_{\mathrm{q}}\theta}\right)\cdot \left(1 - \frac{\lambda V\Delta C}{NG}\right)\right]\right\} \qquad (8a)$$

$$P_{\mathrm{I}} = 1 - \exp\left(-\frac{\eta_{\mathrm{m}}^2 pBNq\theta}{\lambda_{\mathrm{q}}V}\right) \qquad (8b)$$

2.2 Control strategies based on WR models

Based on two WR models, a potential ventilation control strategy is proposed and named NSS/SS-IAQ control.

First, through solving Eqs. (8a) and (8b), the required ventilation rates can be obtained from the NSS/SS WR models (hereafter named as ACH_{NSS} and ACH_{SS}), which reduce the infection risk to a target infection risk. In this study, the basic reproductive number is used to determine the target infection risk, which is the number of secondary infections caused by one infected individual [13, 21]. When the basic reproductive number is less than one, i. e., the number of secondary infections caused by one infected individual is less than one, the disease cannot spread in the population. Therefore, the relationship between target infection risk and initial infection rate is:

$$P_{\mathrm{I}} = \frac{B}{1 - B} \qquad (9)$$

Then, considering that the IAQ must be maintained in real buildings, the ventilation rate cannot be lower than the ventilation for IAQ (the air change rate for ventilation hereafter is referred as ACH_{IAQ}). From Eqs. (5a) and (5b), there is no ventilation demand for preventing transmission when there are no occupants. However, in a real building, outdoor air can be provided to prevent odours, even though there are no occupants [23].

Therefore, a comparison between ACH_{IAQ} and the required ventilation rates from the two WR models should be conducted. Finally, the actual ventilation rate that fulfills the IAQ and target infection risk requirements is obtained (hereafter named $ACH_{\mathrm{NSS-IAQ}}$ and $ACH_{\mathrm{SS-IAQ}}$). Information about the ventilation control strategy for IAQ and new control strategies for both IAQ and infection risk is summarized in Table 1.

Table 1 Comparison of ventilation control strategies based on IAQ and WR models

Control strategy	Corresponding air change rate	Description
IAQ	ACH_{IAQ}	Supplies fresh air based on the IAQ demand.
SS-IAQ	$ACH_{SS\text{-}IAQ}=\max(ACH_{SS}, ACH_{IAQ})$	Supplies fresh air based on the IAQ demand and reduces the infection rate to a target value calculated by SS WR.
NSS-IAQ	$ACH_{NSS\text{-}IAQ}=\max(ACH_{NSS}, ACH_{IAQ})$	Supplies fresh air based on the IAQ demand and reduces the infection rate to a target value calculated by NSS WR.

2.3 Case study

2.3.1 Building and HVAC system

A real 16-storey high-rise institutional building was selected for a case study to analyze infection risk and energy simulation. The air-conditioned volume of this building is about 155000 m³. This occupied period is from 5:00 AM to midnight. The fresh air is supplied by a centralized balanced ventilation system during this occupied period. The current ventilation control strategy is based on the IAQ. For each floor, the CO_2 sensors are installed in the return air ducts. The fresh air flow rate is controlled based on the measured CO_2 concentration. It is constant (around 11.3 m³/s; 0.3 ACH) if the CO_2 concentration is lower than 650×10^{-6}. When the CO_2 concentration is greater than 650×10^{-6}, the fresh air supply rate increases. A maximum fresh air rate (around 35.7 m³/s; 0.8 ACH) is supplied once the CO_2 concentration reaches 850×10^{-6}. The indoor air temperature is maintained at 23 °C.

The major equipment of the ventilation and cooling system is summarized in Table 2. The heating system is also installed, but this study mainly focused on the ventilation and cooling system, and thus the heating system is not investigated. Mathematic models were applied to simulate the power of chillers, pumps, cooling towers, and fans, when the inputs of outdoor conditions, building cooling load, and required ventilation rate are known. The outdoor conditions (outdoor temperature and wet-bulb temperature) and building cooling load were considered as the known inputs, which were measured in the case study building (see Section 2.3.3). The required ventilation rate is based on the new control strategies proposed in Section 2.2. The energy simulation needs to calculate the power demand of fans and pumps, the power of cooling towers, and the cooling load allocated to fresh air and chiller system.

Table 2 Energy models and detailed information about the ventilation and cooling system.

Equipment	Detailed information
Two chillers	Centrifugal chiller capacity and power: 1969 and 347 kW Screw chiller capacity and power: 260 and 62 kW
Four fans and five pumps	Pumps' total nominal power: 105 kW Specific fan power: 3.76 kW/(m³·s⁻¹)
Two cooling towers	Nominal power: 26.8 kW

For the chiller:

$$\frac{1}{COP_i} = \alpha_{0,i} + \alpha_{1,i}\frac{1}{\dot{q}_{ch,i}} + \alpha_{2,i}\dot{q}_{ch,i} + \alpha_{3,i}\frac{T_{ci,i}}{\dot{q}_{ch,i}} +$$
$$\alpha_{4,i}\frac{T_{ci,i}^2}{\dot{q}_{ch,i}} + \alpha_{5,i}T_{ci,i} + \alpha_{6,i}\dot{q}_{ch,i}T_{ci,i} + \alpha_{7,i}T_{ci,i}^2 +$$
$$\alpha_{8,i}\dot{q}_{ch,i}T_{ci,i}^2 \tag{10}$$

$$T_{ci,i} = \beta_{0,i} + \beta_{1,i}T_{wb} + \beta_{2,i}T_{wb}^2 + \beta_{3,i}\dot{q}_{ch,i} + \beta_{4,i}\dot{q}_{ch,i}^2 \tag{11}$$

$$P_{ch} = \sum_i^{N_{ch}}\frac{\dot{q}_{ch,i}}{COP_i} \tag{12}$$

where P_{ch}, COP_i, $\dot{q}_{ch,i}$, $T_{ci,i}$, α_i and β_i represent the power, coefficient of performance, cooling load, condensing water temperature of the ith chiller, and correlation coefficients, respectively.

For fans and pumps:

$$P_{F/P} = \sum_i^{N_{F/P}} P_{F/P,nom,i}\left(\frac{Q_{F/P,i}}{Q_{F/P,nom,i}}\right)^3 \tag{13}$$

$$P_F = SQ \tag{14}$$

$$Q_{w,i} = \gamma_{0,i} + \gamma_{1,i}\dot{q}_{ch,i} + \gamma_{2,i}\dot{q}_{ch,i}^2 + \dot{q}_{ch,i}^3 \tag{15}$$

where $P_{F/P}$, P/Q_{nom}, S, $Q_{w,i}$ and $\gamma_{0,i}$ and γ_i represent the power of fans or pumps, nominal power/flow rate of fans or pumps, specific fan power, water flow rate, and correlation coefficients, respectively. As the results shown in Section 3.1, the ventilation rate under NSS/SS-IAQ control may exceed the existing maximum fan flow rate. When the ventilation rate is

lower than the existing maximum fan flow rate (35.7 m³/s; 0.8 ACH), the fan energy consumption will be calculated using Eq. (13). The fan energy consumption will be calculated using Eq. (14), when the ventilation rate is higher than the existing maximum fan flow rate.

For the cooling towers:

$$P_{CT} = \sum_{i}^{N_{CT}} P_{CT,nom,i} (R_{CT,i})^3 \qquad (16)$$

$$R_{CT,i} = d_{0,i} T_{ci,i} + d_{1,i} \qquad (17)$$

where P_{CT}, $R_{CT,i}$ and d_i represent the power of the cooling tower, the rotation speed ratio, and correlation coefficients, respectively.

The relationships between the building cooling load, fresh air cooling load, and chiller system cooling load are:

$$\dot{q}_{CL} = \dot{q}_{ch} + \dot{q}_{oa} \qquad (18)$$

$$\dot{q}_{oa} = Q\rho_a (c_p \Delta T + h_g \Delta W) \qquad (19)$$

where $\dot{q}_{CL}$, $\dot{q}_{oa}$, Q, ρ_a, c_p, h_g, ΔT and ΔW represent building cooling load, fresh air-cooling load, fresh air flow rate, air density, specific heat, water latent heat, indoor and outdoor temperature, and humidity difference, respectively.

Information about the ventilation and cooling system is briefly listed in Table 2. The other information, including the correlation coefficients and accuracy of the sensors, can be found in previous energy simulation studies conducted by us [24−25]. The validation of these energy models is presented in Section 3.2.2. The key measured data from the centralized HVAC system, such as building cooling load, outdoor temperature and humidity are presented in Section 2.3.3.

The measured data from the CO_2 sensors and fresh airflow rate sensors from the 1st to 15th floors are used to estimate the variation in the number of occupants on each floor and provide a baseline case for IAQ control. All these devices are monitored and controlled by a building automation system (BAS). The detailed data used in this study are introduced in Section 2.3.3.

2.3.2 Ventilation settings

Table 3 lists the input parameters for different ventilation settings. Compared with Case 1, the settings of Cases 2−5 aim to investigate the impacts of quantum generation rate, exposure time,

protective measures, and initial infection rate on ACH_{NSS} and ACH_{SS}. The other two parameters, pulmonary rate (p) and CO_2 generation rate (G), are selected as 0.5 m³/h and 0.0297 m³/h from Ref. [26−27]. The building volume to occupant ratios should also be investigated (See Eqs. (5a) and (5b)).

Table 3 Cases for ventilation calculation

Case	Quantum generation rate/ (q·h⁻¹)	Time/h	Protect measure	Initial infection rate
1	857	2	η_m=0.5, P_d=3.1	0.01
2	500	2	η_m=0.5, P_d=3.1	0.01
3	857	8	η_m=0.5, P_d=3.1	0.01
4	857	2	η_m=1, P_d=1	0.01
5	857	2	η_m=0.5, P_d=3.1	0.1

Note: For each case, three different ratios of building volume to occupant are evaluated, 52, 78 and 155 m³/person, i.e., 100%, 67% and 33% occupancy.

For each case, three different building volume to occupant ratios (here and after referred to as V/N) are evaluated: 52, 78 and 155 m³/person. These three ratios represent 100% occupancy (i. e., this building with 155000 m³ volume is fully occupied by 3000 occupants), 67% occupancy (2000 occupants), and 33% occupancy (1000 occupants). The different initial quantum concentrations based on the CO_2 concentration are also studied. The results are shown in Section 3.1.

Taking COVID-19 as an example, two quantum generation rates are selected. The previous studies show that the quantum generation rates of COVID-19 vary within a large range from 14 to 1190 q/h [17, 28]. In this study, 857 q/h and 500 q/h are chosen to represent the high-risk and moderate-risk scenarios [19]. Since it is difficult to monitor the accurate exposure time for each occupant, the exposure time is selected based on the following assumptions. The reference suggests that a classroom may have a 2-h exposure time [8], which is considered a mild-risk scenario. The standard hours of work for an office building can extend to 8 h in Canada [29]. Although it is rare to continuously stay in a space for 8 h in a real scenario, the 8-h exposure is selected and can be considered the high-risk scenario. Two situations are considered for the protective measures. During the COVID-19 pandemic, public buildings usually enforce a strict rule on wearing masks and social distancing.

Therefore, 50% of the mask filtration efficiency (η_m) and 0.32 social distancing index (2 m social distance) are selected from Refs. [8, 19]. However, in real scenarios, these two protective measures may not be followed. Under the scenario that nobody wears masks, and nobody follows social distancing, both of the mask filtration efficiency and social distancing index are one. For example, wearing masks for many hours may cause headaches and/or breathing difficulties and the development of facial skin lesion [9]. The initial infection rates are developed based on different regions in North America [30].

2.3.3 Data for ventilation and energy consumption simulation

To show the difference of $ACH_{NSS-IAQ}$ and ACH_{SS-IAQ} in the real operation (i. e., based on the NSS/SS-IAQ control in Section 2.2), six months of data (from June to August in 2019 and 2020) were collected from the BAS system. Since the data in 2020 reflect the real energy consumption during the COVID-19 pandemic, they were used to validate the energy models (Section 3.2.2). However, due to the frequent shutdown of this building in 2020, the 2019 data were used to simulate the ventilation and cooling energy consumption (Sections 3.2.1 and 3.2.2). During the shutdown period in 2020, this building was not occupied, hence there is no requirement for infection risk reduction. For the whole measured period (from June to August in 2019 and 2020), the inputs were summarized in Table 4.

A specific day (August 21, 2019 from 5:00 AM) is selected to show the hourly $ACH_{NSS-IAQ}$ and ACH_{SS-IAQ} (Section 3.2.1) and the hourly energy consumption (Section 3.2.2). Figure 2 shows the inputs for the calculation, including the CO_2 concentration variation range, ventilation rate under the current IAQ control, the number of occupants,

building cooling load, outdoor temperature, and humidity on August 21, 2019. The hourly ventilation rate under the current IAQ control, outdoor temperature, and humidity were directly measured by the BAS system. The building cooling loads were calculated from the measured chilled water temperature difference and water flow rate. The BAS system recorded all the CO_2 levels for the 1st – 15th floors. The CO_2 concentration ranges are presented by three values: max, min, and average, which are the measured hourly maximum, minimum, and average CO_2 levels on the 1st – 15th floors.

The number of occupants on each floor was calculated from the measured CO_2 concentration and fresh air supply rate by following an equation that was validated in previous occupancy detection studies [27, 31] .

$$N^n = \frac{V_i(C_{ia}^{n+1} - C_{ia}^n)}{G \Delta t} + \frac{V_i \lambda_i^n (C_{ia}^n - C_{oa}^n)}{G} \tag{20}$$

where the superscript n represents the current step; the subscript i represents the indoor spaces (i. e., floors 1 – 15 in this study); G is the CO_2 generation rate per person, 0.0297 m^3/h; V_i is the ith indoor space volume, m^3; C_{ia}^n is the CO_2 concentration in the indoor space at time n, 10^{-6}; C_{oa}^n is the outdoor CO_2 concentration at time n, which is assumed to be constant at 400×10^{-6} [27]; Δt is the time step, 0.1 h.

A high initial quantum concentration scenario is also considered, where the CO_2 level is 1000×10^{-6} at 5:00 AM [32 – 33]. A ventilation failure may lead to a very high CO_2 level before occupants enter the building [34]. For example, in the European Heating and Ventilating Associations Guidebook 13, the upper limit for the CO_2 level is 1500×10^{-6} in schools [32]. The results in Section 3.1 show that the initial quantum concentration (i. e., CO_2 concentration) has a great impact on the ACH_{NSS}. However, because the IAQ control usually limits the maximum CO_2 level

Table 4 Summary of the measured data

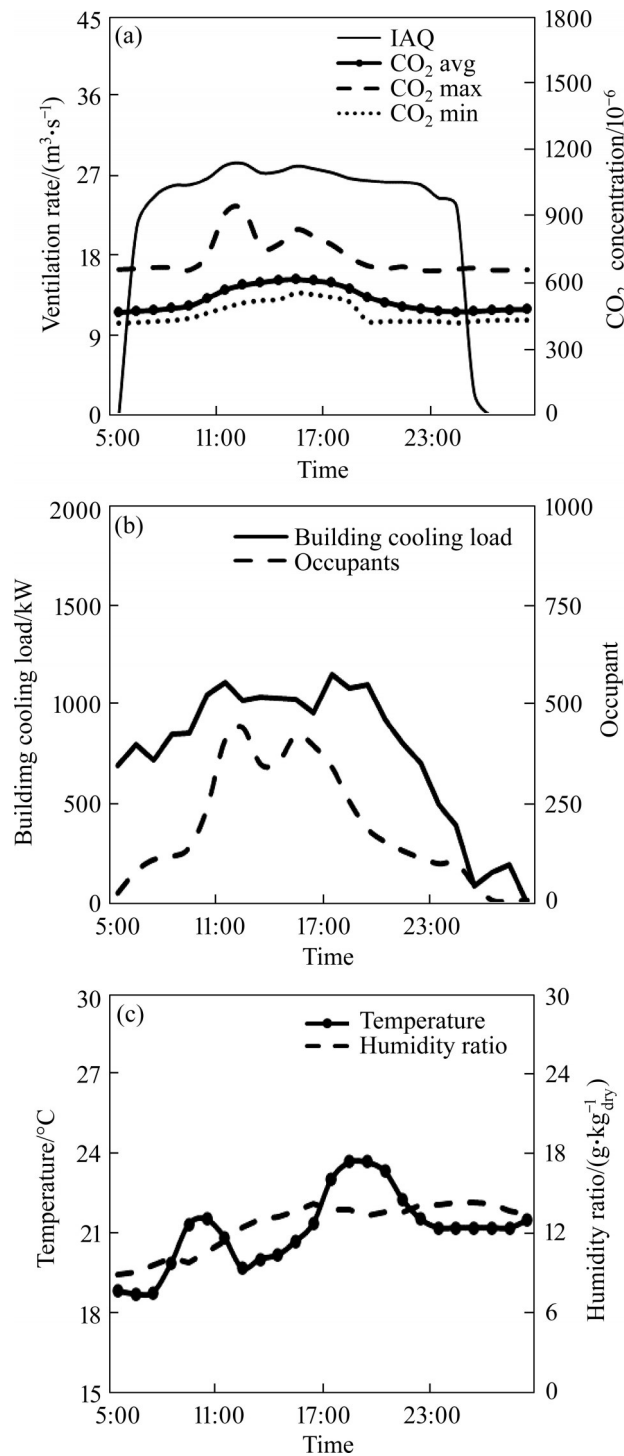| Year	Level	Temperature/°C	Humidity ratio/($g \cdot kg_{dry}^{-1}$)	Hourly occupant	CO_2 concentration/10^{-6}	Cooling load/kW
	Min	8	3	2	386	0
2019	Avg	22	9	113	480	654
	Max	32	16	669	1142	1369
	Min	7	4	—	—	0
2020	Avg	22	10	—	—	601
	Max	34	18	—	—	1336

Figure 2 Measured data for a specific day: (a) Building CO_2 variation range and ventilation rates based on the IAQ control; (b) Building cooling load and the number of occupants; (c) Outdoor temperature and humidity ratio

in this building to lower than 1000×10^{-6} (see Figure 2(a)), the difference between the hourly $ACH_{NSS\text{-}IAQ}$ and $ACH_{SS\text{-}IAQ}$ is small. A high initial quantum concentration scenario is used to highlight the difference between $ACH_{NSS\text{-}IAQ}$ and $ACH_{SS\text{-}IAQ}$.

3 Results and discussion

3.1 Parametric study on required ventilation rates

Figure 3 presents and compares ACH_{NSS} and ACH_{SS} under different cases (see Table 2). Figure 3(a) shows that the initial quantum concentration greatly impacts ACH_{NSS}. When the initial quantum concentration, $C_{q,0}$, is zero, ACH_{NSS} is obviously lower than λ_{SS}. However, when $C_{q,0}$ increases, ACH_{NSS} increases quickly, and is greater than ACH_{SS} when $C_{q,0}$ is around 0.02 q/m^3 (400×10^{-6}). Also, when the number of occupants decreases, the difference between ACH_{NSS} and ACH_{SS} increases. For example, when the initial quantum concentration is zero, the difference between the NSS/SS WR models increases from 0.19 ACH to 0.28 ACH when the building volume to occupant ratio (V/N) increases from 52 to 155 m^3/person.

By comparing Figures 3(a) and (b), it can be seen that when the quantum generation rate, q, decreases, the difference between ACH_{NSS} and ACH_{SS} increases. For example, when $V/N=$ 52 m^3/person, the difference between ACH_{NSS} and ACH_{SS} is 0.22 ACH when q is 500 q/h, vs. 0.19 ACH when q is 857 q/h. Also, it should be noted that in Case 2, when there are fewer than 1000 occupants and $C_{q,0}$ is lower than 0.005 q/m^3 (see Figure 3(b), $V/N=155$ m^3/person), ACH_{NSS} is close to zero. This indicates that the infection risk is low enough even without ventilation. Figure 3(c) shows that the increased exposure time shrinks the difference between the NSS/SS models. For example, when the exposure time increases from 2 h to 8 h, the biggest difference between ACH_{NSS} and ACH_{SS} reduces from 0.19 ACH at zero $C_{q,0}$ to 0.04 ACH. This shrinkage is calculated using Eqs. (8a) and (8b). Without considering the effects of the initial virus concentration, Eq. (8a) will be equal to Eq. (8b) for an infinite exposure time. In other words, with the same target infection risk, as the exposure time increases, ACH_{NSS} will be closer to ACH_{SS}.

Figure 3(d) shows that the protective measures (i.e., wearing masks and social distancing) significantly affect the required ventilation rates. When $C_{q,0}$ is zero, the difference between ACH_{NSS} and ACH_{SS} can reach 0.6 ACH, which is higher than
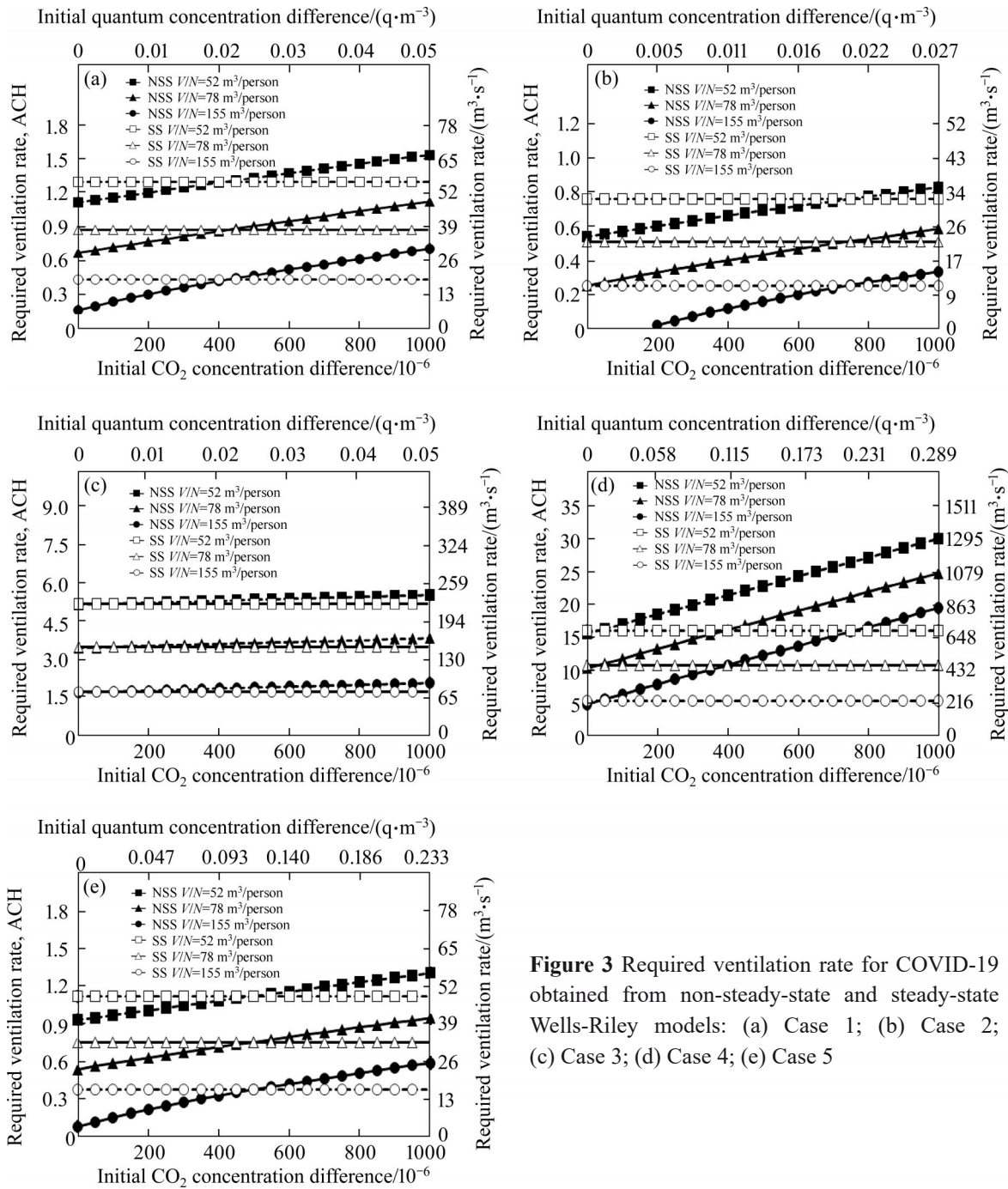
Figure 3 Required ventilation rate for COVID-19 obtained from non-steady-state and steady-state Wells-Riley models: (a) Case 1; (b) Case 2; (c) Case 3; (d) Case 4; (e) Case 5

that in Case 1 (see Figure 3(a)). Without the protective measures, $C_{q,0}$ has a significant impact on ACH_{NSS}. When $C_{q,0}$ is around 0.3 q/m³ (around 1000× 10⁻⁶), the ventilation difference between the NSS/SS models goes up to 14 ACH, which is much greater than the difference in the other four cases (Cases 1– 3 and 5). This is because the function of the protective measures is to reduce the amount of virus in the air. Without the protective measures, the virus needs to be completely removed by ventilation (i.e., the amount of virus that needs to be removed is

greater without protective measures). Therefore, with a high $C_{q,0}$, ACH_{NSS} is much higher than ACH_{SS}. However, the effects of initial infection rates on the ventilation difference between the NSS/SS models are slight. Figure 3(e) shows that the difference is close to the difference presented in Figure 3(a). For example, under the conditions of V/N=52 m³/person and $C_{q,0}$=0, the differences between ACH_{NSS} and ACH_{SS} are both around 0.19 ACH for Case 1 and Case 5. In Eqs. (8a) and (8b), the change in the initial infection rate, B, will not change the term that

has the main difference between Eqs. (8a) and (8b).

From Figure 3, the main difference between ACH_{NSS} and ACH_{SS} depends on the initial quantum concentration, $C_{q,0}$. When $C_{q,0}$ is high, the ACH_{NSS} can be much larger than the ACH_{SS}, e.g., in Figure 3(d), the ACH_{SS} is fixed at 16, 11 and 5ACH, while ACH_{NSS} reaches 30, 25 and 20 ACH when the $C_{q,0}$ reaches 0.3 q/m³. Using the NSS WR model is safer than the SS WR model, because the impact of $C_{q,0}$ is considered in the NSS WR model (see Eq. (8b)), and the existence of $C_{q,0}$ increases the infection risks.

To highlight this point and analyze the risk, the actual infection risk of ACH_{SS} under a NSS condition is presented in Figure 4 based on Case 4 settings (i.e., substitute the ACH_{SS} in Figure 3(d) into the NSS WR model, Eqs. (5a) and (8a)). Figure 4 shows that when $C_{q,0}$ is higher than zero, the actual infection risk is higher than the target value. This result indicates that it is better to use the NSS WR model to control mechanical ventilation systems; Otherwise, the infection risk cannot be controlled ideally. For example, when $C_{q,0}$ is 0.3 q/m³, the actual infection risk under $ACH_{SS}=5$ condition is 3.5%, which is higher than the target infection risk (1%).
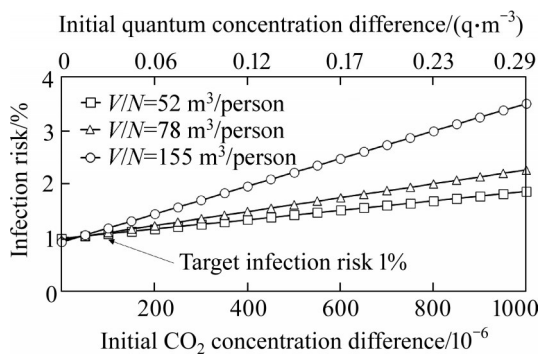

Figure 4 Actual infection risk of ACH_{SS} in Case 4

These results match the previous studies, and further showed that the difference of required ventilation rates between NSS/SS WR models can reach extremely high (up to 14ACH) under some cases. In the previous study, HARRICHANDRA et al [16] estimated the infection risk for 12 nail salons by using both NSS/SS conditions. Two scenarios were considered, NSS/SS scenarios, and the exposure time in the NSS scenarios (2.5 h) was longer than in the SS scenarios (1 h). It was found that the infection risk calculated from the SS WR model was 20% higher than that from the NSS WR model. However, this study did not investigate the NSS/SS WR models under the same conditions and did not analyze the impacts of different factors, such as social distancing, on the required ventilation rates calculated by the NSS/ SS WR models.

In this study, in Figure 3(b), when the initial quantum concentration, $C_{q,0}$, is zero, ACH_{NSS} is obviously lower than ACH_{SS}. This result indicates that the SS WR model overestimates the infection risk under the conditions of Case 2, matching the results in Ref. [16]. In Figure 3(d), ACH_{NSS} is higher than ACH_{SS} when the $C_{q,0}$ is 0.288 q/m³. This result indicates that the SS WR model underestimates the infection risk under the conditions of Case 4 with a high $C_{q,0}$

3.2 Effects of control strategies on required ventilation rates and energy consumption

3.2.1 Effects of control strategies on required ventilation rates

The specific day (August 21, 2019) is used to show the ventilation rates under the NSS/SS-IAQ control. Two representative ventilation settings, Case 1 and Case 4, are selected for calculating ACH_{NSS} and ACH_{SS}. As shown in Section 3.1, Case 1 shows a large relative difference at zero $C_{q,0}$, and Case 4 can have a large difference on ACH_{NSS} and ACH_{SS} when $C_{q,0}$ increases. Figure 5 presents the hourly $ACH_{NSS-IAQ}$ and ACH_{SS-IAQ} under the Case 1 and Case 4 settings on the specific day. Under Case 1 setting, the values of $ACH_{NSS-IAQ}$ and ACH_{SS-IAQ} are almost the same. The largest relative difference is less than 10% between $ACH_{NSS-IAQ}$ and ACH_{SS-IAQ} at a very low ventilation rate (around 1 m³/s) during the night. By comparing with ACH_{IAQ} in Figure 2(a), it can be found that $ACH_{NSS-IAQ}$ and ACH_{SS-IAQ} are individually equal to ACH_{IAQ}, indicating that ACH_{IAQ} dominates the ventilation control. This is caused by the low number of occupants. In Figure 2(b), at the highest point, V/N is around 350, which leads to much lower ACH_{NSS} and ACH_{SS} than ACH_{IAQ}. Therefore, ACH_{IAQ} is sufficient to fulfill the safety requirement without extra ventilation rates.

Compared with Case 1 (Figure 5(a)), Figure 5(b) shows that the relative difference in Case 4 is higher than that in Case 1. However, the absolute difference in the ventilation rate is small,
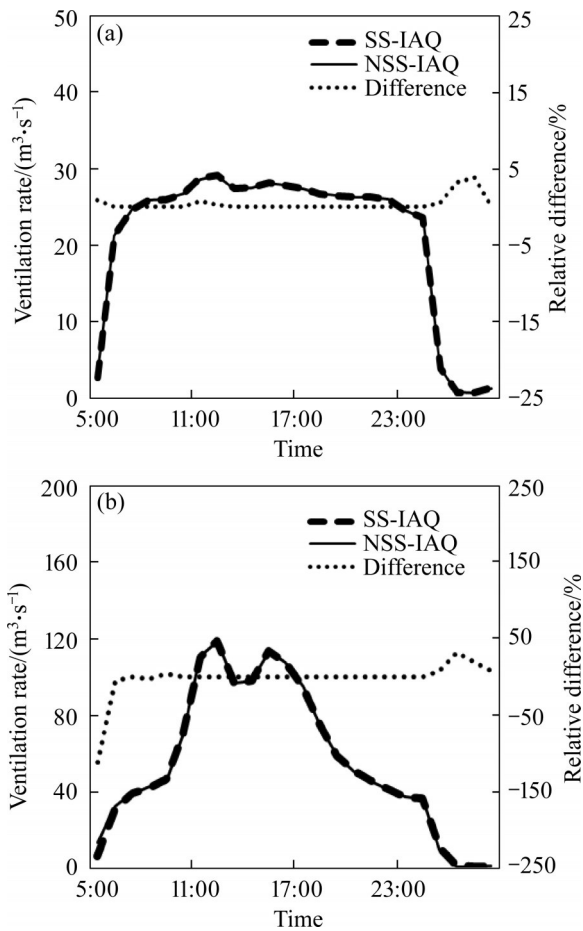
Figure 5 Ventilation rates and relative difference under the measured scenario on the specific day: (a) Case 1; (b) Case 4

Figure 6 Ventilation rates and relative difference under a high initial quantum concentration scenario on the specific day: (a) Case 1; (b) Case 4

because the difference of $ACH_{NSS-IAQ}$ and ACH_{SS-IAQ} exists only when the ventilation rate is low. During the morning, $ACH_{NSS-IAQ}$ is higher than ACH_{SS-IAQ}. The largest relative difference appears at 5:00 AM, when $ACH_{NSS-IAQ}$ (14 m^3/s; 0.3 ACH) is around twice that of ACH_{SS-IAQ} (6.7 m^3/s; 0.16 ACH). During the afternoon and evening, $ACH_{NSS-IAQ}$ is lower than ACH_{SS-IAQ}, with about a 1 m^3/s (around 30%) difference.

Figure 6 presents $ACH_{NSS-IAQ}$ and ACH_{SS-IAQ} calculated from Case 1 and Case 4 under a high initial quantum concentration scenario (See 2.3.3). In Figure 6(a), the difference between ACH_{NSS} and ACH_{SS} remains small. However, in Figure 6(b), for three hours during the morning (5:00 AM to 8:00 AM), the difference between $ACH_{NSS-IAQ}$ and ACH_{SS-IAQ} is very big, reaching 36 m^3/s and $ACH_{NSS-IAQ}$ is three times higher than ACH_{SS-IAQ} at the highest points. Whereas, in the afternoon and evening, the difference between $ACH_{NSS-IAQ}$ and
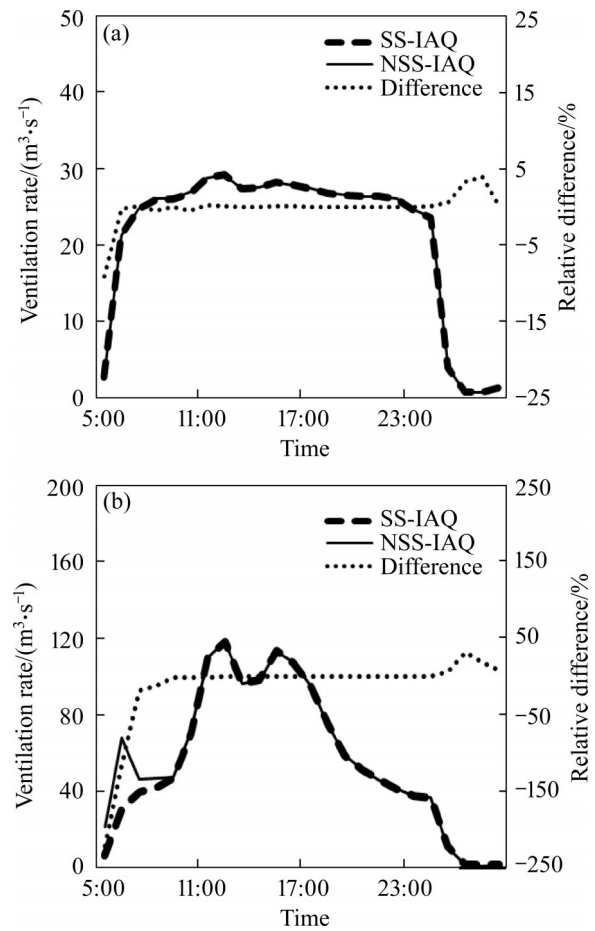
ACH_{SS-IAQ} remains small. This change can be explained by Figures 3(a) and (d). Since the NSS WR model in Case 1 is not sensitive to the initial quantum concentration, a high initial quantum concentration cannot lead to a large difference. In Case 4, a high initial quantum concentration will cause a huge increase in ACH_{NSS}. However, due to an initial high ventilation rate, the quantum concentration in the building (i.e., CO_2 concentration in the building) reduces quickly and the difference between $ACH_{NSS-IAQ}$ and ACH_{SS-IAQ} continues to shrink.

The results in Figures 5 and 6 highlight the IAQ effects on the two new ventilation control strategies (i.e., NSS-IAQ/SS-IAQ control strategies). Under the existing ventilation control strategy based on IAQ, the difference between $ACH_{NSS-IAQ}$ and ACH_{SS-IAQ} is quite small, because this strategy limits the building CO_2 level to around 460×10^{-6} (i.e., a low initial quantum concentration).

However, assuming that all floors have initial 1000×10^{-6} CO_2 concentration, $ACH_{NSS-IAQ}$ is much higher than ACH_{SS-IAQ}, indicating that the SS WR model may underestimate the ventilation rate.

These results indicate that it is safer to use the NSS WR model in the ventilation control since it considers the initial concentration. Also, it is important to keep the building at a low CO_2 level even it is not occupied.

3.2.2 Effects of control strategies on energy consumption

This section presents the impacts of new ventilation control strategies (Section 2.2.) on energy consumption. The setup and boundary conditions of the simulation are presented in Section 2.3. This section begins with validation of the energy models. Figure 7 presents the difference between the measured and calculated energy consumption of the chiller and ventilation systems from June to August 2020. The largest relative error for the chiller system and fans was 2.8% (August) and 8.5% (June) respectively, but both were lower than the suggested relative error of 15% in the Ref. [35]. The accuracy of the energy models was also evaluated by the hourly CV(RMSE) and NMBE. According to ASHRAE guideline-14, the hourly CV(RMSE) and NMBE between measurement and simulation should be less than 30% and ±10% respectively [36]. In this study, the hourly CV(RMSE) and NMBE of the chiller system were 7% and 2%, and the hourly CV(RMSE) and NMBE of the fans were 15% and 2%; these are lower than the values in ASHRAE guideline-14. Therefore, the energy models are validated.
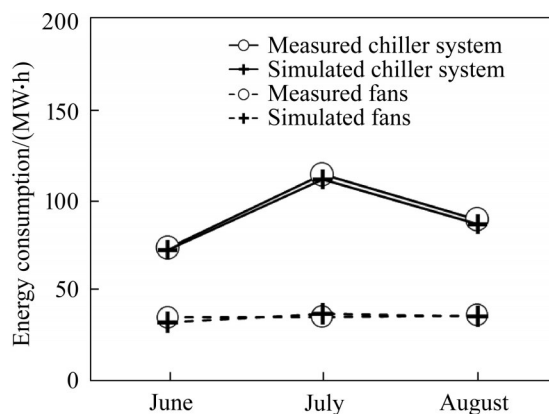
Figure 7 Difference between monthly measured ventilation and cooling energy usage and simulated ventilation and cooling energy usage during the COVID-19 pandemic in 2020

Figure 8 presents the ventilation and chiller cooling energy consumption based on $ACH_{NSS-IAQ}$ and ACH_{SS-IAQ} of Case 4 with a high initial quantum concentration on the specific day. The differences between NSS/SS-IAQ control strategies on ventilation and chiller cooling energy consumption are significant during the morning. For example, the ventilation energy consumption of the NSS-IAQ control strategy is 125 kW·h higher than that of the SS-IAQ control strategy at 6:00 AM. However, the cooling energy consumption under the NSS-IAQ control strategy is 23.5 kW·h lower than that under the SS-IAQ control strategy due to the difference between $ACH_{NSS-IAQ}$ and ACH_{SS-IAQ}. Higher $ACH_{NSS-IAQ}$ leads to a higher ventilation energy consumption than the ventilation energy consumption under SS-IAQ control strategy. However, in Figure 2(b), during the morning, the outdoor temperature and humidity ratio are lower than the indoor environment setpoints (23 °C and 11.6 g/kg$_{dry}$). The
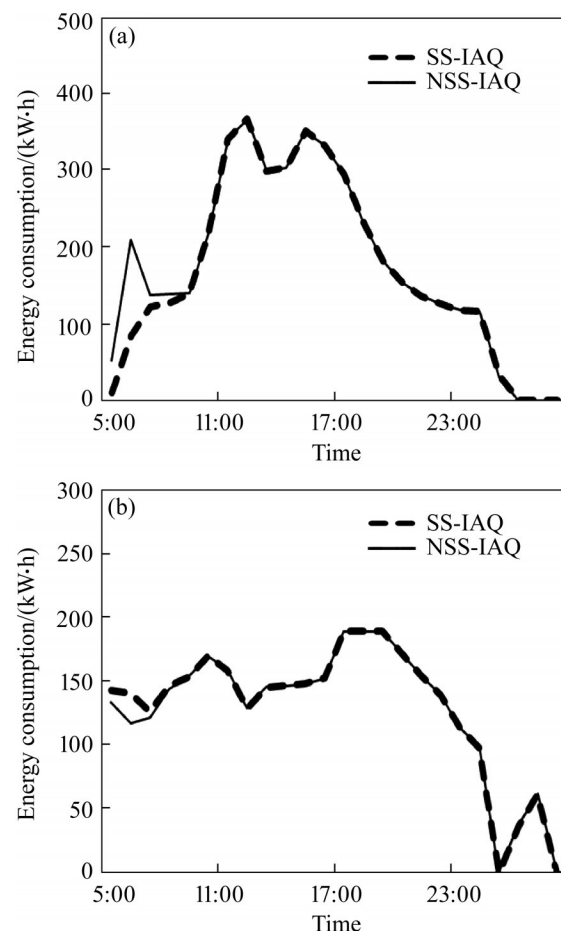
Figure 8 Energy consumption between SS-IAQ and NSS-IAQ control strategies of Case 4 with a high initial quantum concentration on the specific day: (a) Ventilation; (b) Chiller cooling

high ventilation rate introduces more outdoor cool air into the building, and thus reduces the cooling loads for the chiller system.

Figure 9 evaluates the total energy consumption difference between NSS/SS-IAQ control strategies in Case 1 and Case 4 from June to August in 2019 (Note: No high initial quantum concentration). For comparison, the energy consumption with only IAQ control is also presented. The different long-term effects between NSS/SS-IAQ on the required ventilation rate and chiller cooling energy consumption are small. For example, the ventilation energy consumption of the NSS-IAQ control strategy is only around 1% lower than that of the SS-IAQ control strategy in Case 4, while there is almost no difference on the chiller cooling energy consumption for these two control strategies. Figure 5 shows that the difference between $ACH_{NSS-IAQ}$ and ACH_{SS-IAQ} is small due to the low initial quantum concentration limited by IAQ control. Section 3.1 explained that when the initial quantum concentration is zero, ACH_{NSS} can be

slightly lower than ACH_{SS}. Therefore, in the long-term case study operation, the differences between NSS/SS-IAQ control strategies on the required ventilation rate and chiller cooling energy consumption are small. These results indicate that the building IAQ should be well controlled, e.g., the indoor CO_2 level is maintained below $460×10^{-6}$ in the case study.

From the results in Figures 5, 6 and 8, only when the occupants do not have any protective measures (e.g., Case 4) and the initial quantum concentration is high, the difference between $ACH_{NSS-IAQ}$ and ACH_{SS-IAQ} is large. The ventilation energy consumption between $ACH_{NSS-IAQ}$ and ACH_{SS-IAQ} has a relatively large difference. For the other settings (e.g., Case 1), the difference between $ACH_{NSS-IAQ}$ and ACH_{SS-IAQ} is small. From Eq. (5a) and Eq. (5b), the main difference between the NSS/SS WR model is related to the protective measures and initial quantum concentration. In summary, the difference between $ACH_{NSS-IAQ}$ and ACH_{SS-IAQ} depends on the situation. The results of Figure 4 indicate that the NSS WR model is safer than the SS WR model, because the ACH_{SS} cannot reduce the actual infection risk to the target value in Case 4. Therefore, the NSS WR model is more recommended for the ventilation control strategy.

4 Conclusions

This paper first investigated the differences between the non-steady-state (NSS) and steady-state (SS) Wells-Riley (WR) models. The NSS/SS WR models were established, which included factors that were ignored in the previous study, such as the initial quantum concentration. Then, two new ventilation control strategies based on the NSS/SS WR models were proposed. Using a real building for the case study, the differences in the ventilation rates and energy consumption under the two new ventilation control strategies were evaluated. The major conclusions are summarized below:

1) Without considering the initial quantum concentration, the required ventilation rate calculated with the NSS WR model is always lower than the required ventilation rate calculated with the SS WR model, but the difference is small. For this study, the largest difference reached 0.6 ACH.

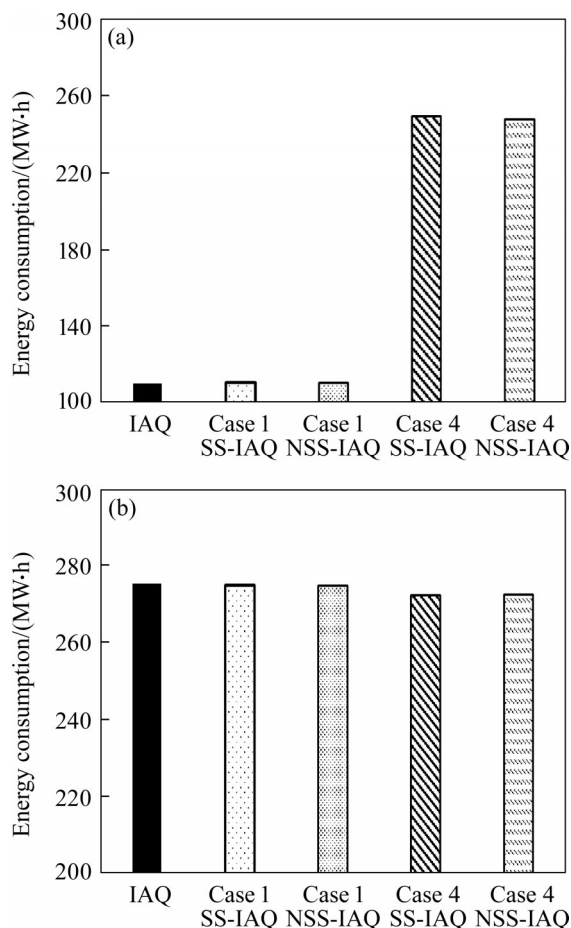2) If the occupants do not follow any protective

Figure 9 Energy consumption differences between ventilation settings: (a) Ventilation; (b) Chiller cooling

measures (e.g., wearing masks and social distancing), the high initial quantum concentration can lead to large differences between the NSS/SS WR models for the required ventilation rate, which indicates that the SS WR model may underestimate the ventilation rate required to reduce the risk of infection. In the case study, under a 0.3 q/m^3 initial quantum concentration condition (i.e., CO_2 concentration of 1400×10^{-6}), the required ventilation rate calculated with the NSS WR model was 14 ACH (607 m^3/s) higher than that calculated with the SS WR model.

3) It is recommended to keep the building at a low CO_2 level even it is not occupied. In the case study, if the initial CO_2 concentration is 1000×10^{-6} before occupants enter the building and without protective measures, it will lead to a large difference in the required ventilation rate (36 m^3/s; up to 220%) and related ventilation energy consumption (125 kW·h; up to 150%) between NSS/SS WR controls. However, if the initial CO_2 concentration is 450×10^{-6} before occupants enter the building, the difference is very negligible.

This study focuses on the difference between the NSS/SS WR models. Some methods that can further improve the prediction accuracy of WR models are not considered. For example, it is easy to integrate the new coefficients to improve the WR model and consider the spatial effects. Furthermore, this study only discusses ventilation and cooling energy consumption. During the winter when the outdoor temperature is low, the impacts of the ventilation control strategies based on the WR models on the heating energy consumption should be investigated future.

Contributors

SHA Hao-han wrote the first draft of the manuscript. ZHANG Xin conducted the literature review. QI Da-hai provided the concept and edited the draft of manuscript. SHA Hao-han and QI Da-hai replied to reviewers' comments and revised the final version.

Conflict of interest

SHA Hao-han, ZHANG Xin, and QI Da-hai declare that they have no conflict of interest.

References

[1] World Health Organization (WHO). Coronavirus disease (COVID-19) pandemic-2021 [OL]. [2021-09-12]. https://www.who.int/emergencies/diseases/novel-coronavirus-2019.

[2] FENG Yu, MARCHAL T, SPERRY T, et al. Influence of wind and relative humidity on the social distancing effectiveness to prevent COVID-19 airborne transmission: A numerical study [J]. Journal of Aerosol Science, 2020, 147: 105585. DOI:10.1016/j.jaerosci.2020.105585.

[3] SETTI L, PASSARINI F, de GENNARO G, et al. Airborne transmission route of COVID-19: Why 2 meters/6 feet of inter-personal distance could not be enough? [J]. International Journal of Environmental Research and Public Health, 2020, 17(8): 2932. DOI: 10.3390/ijerph17082932.

[4] MORAWSKA L, TANG J W, BAHNFLETH W, et al. How can airborne transmission of COVID-19 indoors be minimised? [J]. Environment International, 2020, 142: 105832. DOI: 10.1016/j.envint.2020.105832.

[5] GREENHALGH T, JIMENEZ J L, PRATHER K A, et al. Ten scientific reasons in support of airborne transmission of SARS-CoV-2 [J]. Lancet (London, England), 2021, 397(10285): 1603 – 1605. DOI: 10.1016/S0140-6736(21)00869-2.

[6] SHA Hao-han, QI Da-hai. A review of high-rise ventilation for energy efficiency and safety [J]. Sustainable Cities and Society, 2020, 54: 101971. DOI: 10.1016/j.scs.2019.101971.

[7] LUONGO J C, FENNELLY K P, KEEN J A, et al. Role of mechanical ventilation in the airborne transmission of infectious agents in buildings [J]. Indoor Air, 2016, 26(5): 666−678. DOI: 10.1111/ina.12267.

[8] DAI Hui, ZHAO Bin. Association of the infection probability of COVID-19 with ventilation rates in confined spaces [J]. Building Simulation, 2020, 13(6): 1321 – 1327. DOI: 10.1007/s12273-020-0703-5.

[9] SCHIBUOLA L, TAMBANI C. High energy efficiency ventilation to limit COVID-19 contagion in school environments [J]. Energy and Buildings, 2021, 240: 110882. DOI: 10.1016/j.enbuild.2021.110882.

[10] HOU Dan-lin, KATAL A, WANG L . Bayesian calibration of using CO_2 sensors to assess ventilation conditions and associated COVID-19 airborne aerosol transmission risk in schools [J]. MedRxiv, 2021, DOI: 10.1101/2021.01.29.21250791.

[11] REHVA. REHVA COVID-19 guidance document version 4.0.2020 [R].

[12] ZHANG Sheng, LIN Zhang. Dilution-based evaluation of airborne infection risk—Thorough expansion of Wells-Riley model [J]. Building and Environment, 2021, 194: 107674. DOI: 10.1016/j.buildenv.2021.107674.

[13] SZE TO G N, CHAO C Y H. Review and comparison between the Wells-Riley and dose-response approaches to risk assessment of infectious respiratory diseases [J]. Indoor Air, 2010, 20(1): 2 – 16. DOI: 10.1111/j.1600-0668.2009.00621.x.

[14] AGANOVIC A, BI Yang, CAO Guang-yu, et al. Estimating the impact of indoor relative humidity on SARS-CoV-2 airborne transmission risk using a new modification of the

Wells-Riley model [J]. Building and Environment, 2021, 205: 108278. DOI: 10.1016/j.buildenv.2021.108278.

[15] GUO Yong, QIAN Hua, SUN Zhi-wei, et al. Assessing and controlling infection risk with Wells-Riley model and spatial flow impact factor (SFIF) [J]. Sustainable Cities and Society, 2021, 67: 102719. DOI: 10.1016/j.scs.2021.102719.

[16] HARRICHANDRA A, IERARDI A M, PAVILONIS B. An estimation of airborne SARS-CoV-2 infection transmission risk in New York City nail salons [J]. Toxicology and Industrial Health, 2020, 36(9): 634－643. DOI: 10.1177/074 8233720964650.

[17] MILLER S L, NAZAROFF W W, JIMENEZ J L, et al. Transmission of SARS-CoV-2 by inhalation of respiratory aerosol in the Skagit Valley Chorale superspreading event [J]. Indoor Air, 2021, 31(2): 314－323. DOI: 10.1111/ina. 12751.

[18] YANG Wan, MARR L C. Dynamics of airborne influenza A viruses indoors and dependence on humidity [J]. PLoS One, 2011, 6(6): e21481. DOI: 10.1371/journal.pone.0021481.

[19] SUN Chan-juan, ZHAI Zhi-qiang. The efficacy of social distance and ventilation effectiveness in preventing COVID-19 transmission [J]. Sustainable Cities and Society, 2020, 62: 102390. DOI: 10.1016/j.scs.2020.102390.

[20] PENG Zhe, JIMENEZ J L. Exhaled CO_2 as a COVID-19 infection risk proxy for different indoor environments and activities [J]. Environmental Science & Technology Letters, 2021, 8(5): 392−397. DOI: 10.1021/acs.estlett.1c00183.

[21] RUDNICK S N, MILTON D K. Risk of indoor airborne infection transmission estimated from carbon dioxide concentration [J]. Indoor Air, 2003, 13(3): 237－245. DOI: 10.1034/j.1600-0668.2003.00189.x.

[22] ISSAROW C M, MULDER N, WOOD R. Modelling the risk of airborne infectious disease using exhaled air [J]. Journal of Theoretical Biology, 2015, 372: 100－106. DOI: 10.1016/j. jtbi.2

[23] ASHRAE Standard 62.1. Ventilation for acceptable indoor air quality [S].

[24] SHA Hao-han, QI Da-hai. Investigation of mechanical ventilation for cooling in high-rise buildings [J]. Energy and Buildings, 2020, 228: 110440. DOI: 10.1016/j.enbuild.2020. 110440.

[25] SHA Hao-han, MOUJAHED M, QI Da-hai. Machine learning-based cooling load prediction and optimal control for mechanical ventilative cooling in high-rise buildings [J]. Energy and Buildings, 2021, 242: 110980. DOI: 10.1016/j. enbuild.2021.110980.

[26] Health Canada. General exposure factor inputs for dietary,

occupational, and residential exposure assessments [R]. 2014: 52. DOI: https://doi.org/H113-13/2014-1E-PDF.

[27] NG M O, QU Ming, ZHENG Peng-xuan, et al. CO_2-based demand controlled ventilation under new ASHRAE Standard 62.1-2010: A case study for a gymnasium of an elementary school at West Lafayette, Indiana [J]. Energy and Buildings, 2011, 43(11): 3216−3225. DOI: 10.1016/j. enbuild. 2011. 08.021.

[28] BUONANNO G, STABILE L, MORAWSKA L. Estimation of airborne viral emission: Quanta emission rate of SARS-CoV-2 for infection risk assessment [J]. Environment International, 2020, 141: 105794. DOI: 10.1016/j. envint. 2020.105794.

[29] Government of Canada. Hours of work 2020 [OL]. [2021-03-07] https://www.canada.ca/en/employment-social-development/ programs/employment-standards/work-hours.html.

[30] KATAL A, ALBETTAR M, WANG L. City reduced probability of infection (CityRPI) for indoor airborne transmission of SARS-CoV-2 and urban building energy impacts [J]. MedRxiv, 2021: 2021.01.19.21250046.

[31] WANG Sheng-wei, BURNETT J, CHONG H. Experimental validation of CO_2-based occupancy detection for demand-controlled ventilation [J]. Indoor and Built Environment, 1999, 8(6): 377−391. DOI: 10.1177/1420326x9900800605.

[32] ASIF A, ZEESHAN M, JAHANZAIB M. Indoor temperature, relative humidity and CO_2 levels assessment in academic buildings with different heating, ventilation and air-conditioning systems [J]. Building and Environment, 2018, 133: 83−90. DOI: 10.1016/j.buildenv.2018.01.042.

[33] AI Z T, MAK C M. Short-term mechanical ventilation of air-conditioned residential buildings: A general design framework and guidelines [J]. Building and Environment, 2016, 108: 12−22. DOI: 10.1016/j.buildenv.2016.08.016.

[34] CHAN W R, LI Xi-wang, SINGER B C, et al. Ventilation rates in California classrooms: Why many recent HVAC retrofits are not delivering sufficient ventilation [J]. Building and Environment, 2020, 167: 106426. DOI: 10.1016/j. buildenv.2019.106426.

[35] RAHMAN M M, RASUL M G, KHAN M M K. Energy conservation measures in an institutional building in sub-tropical climate in Australia [J]. Applied Energy, 2010, 87(10): 2994−3004. DOI: 10.1016/j.apenergy.2010.04.005.

[36] ASHRAE. ASHRAE guideline 14-2014 measurement of energy, demand, and water savings [M]. Atlana, GA, USA: American Society of Heating, Refrigerating and Air-Conditioning Engineers (ASHRAE), 2014.

(Edited by YANG Hua)

中文导读

<div style="text-align:center">

基于非稳态和稳态 Wells-Riley 模型的机械通风控制策略对于
疾病空气传播和建筑能耗的影响

</div>

摘要：通风是一种有效提高室内空气质量和降低疾病通过空气传播的方法。足量的通风可以降低疾病传播风险，但过量的通风会提高建筑能耗。通风策略需要兼顾这两方面。Wells-Riley(WR)模型常用于预测感染风险和控制通风。但很少有研究对比非稳态和稳态 WR 模型应用在通风策略上的区别。为了填补这一空白，本文探究了基于非稳态和稳态 WR 模型的通风策略对于防疫和建筑能耗的影响。首先，对常用的非稳态和稳态 WR 模型进行改进。一些之前被忽略的参数被加入到 WR 模型中，例如起始病毒浓度。然后，基于非稳态和稳态 WR 模型，提出并对比了两种通风策略。最后，将一栋位于加拿大的建筑物选作案例进行结果展示。案例显示，当起始病毒浓度较高(0.3 q/m³)且室内人员无其他保护措施时，基于稳态 WR 模型的通风策略会低估所需要的通风量。此时，非稳态 WR 模型通风策略的能耗可达稳态 WR 模型通风策略的 2.5 倍。

关键词：建筑通风；Wells-Riley 模型；建筑能耗；空气传播